

A Bayesian approach to the semi-analytic model of galaxy formation: methodology

Yu Lu^{1,2*}, H.J. Mo¹, Martin D. Weinberg¹, Neal Katz¹

¹ *Department of Astronomy, University of Massachusetts, Amherst, MA 01003-9305, USA*

² *Kavli Institute for Particle Astrophysics and Cosmology, Stanford, CA 94309, USA*

ABSTRACT

We believe that a wide range of physical processes conspire to shape the observed galaxy population but we remain unsure of their detailed interactions. The semi-analytic model (SAM) of galaxy formation uses multi-dimensional parameterisations of the physical processes of galaxy formation and provides a tool to constrain these underlying physical interactions. Because of the high dimensionality, the parametric problem of galaxy formation may be profitably tackled with a Bayesian-inference based approach, which allows one to constrain theory with data in a statistically rigorous way. In this paper we develop a SAM in the framework of Bayesian inference. We show that, with a parallel implementation of an advanced Markov-Chain Monte-Carlo algorithm, it is now possible to rigorously sample the posterior distribution of the high-dimensional parameter space of typical SAMs. As an example, we characterise galaxy formation in the current Λ CDM cosmology using the stellar mass function of galaxies as an observational constraint. We find that the posterior probability distribution is both topologically complex and degenerate in some important model parameters, suggesting that thorough explorations of the parameter space are needed to understand the models. We also demonstrate that because of the model degeneracy, adopting a narrow prior strongly restricts the model. Therefore, the inferences based on SAMs are conditional to the model adopted. Using synthetic data to mimic systematic errors in the stellar mass function, we demonstrate that an accurate observational error model is essential to meaningful inference.

Key words: methods: numerical methods: statistical galaxies: evolution galaxies: formation galaxies: luminosity function, mass function.

1 INTRODUCTION

In our current paradigm of structure formation, the matter density of the Universe is dominated by cold dark matter (hereafter CDM), and galaxy formation is a two-stage process (e.g. White & Rees 1978). First, small perturbations in the density field, originating from quantum fluctuations in the early universe, grow and produce a population of virialised dark matter halos. Second, the baryonic matter associated with these halos accumulates at the halo centres owing to cooling and cold flows, forming stars and galaxies. Because of the hierarchical nature of structure formation in a CDM cosmogony, dark matter halos merge. The halo mergers eventually lead to galaxy-galaxy mergers, resulting in the formation of elliptical galaxies.

The first stage of this process, the formation and virialisation of dark matter halos, has been studied in great detail using the (extended) Press-Schechter formalism (e.g. Press & Schechter 1974; Bond et al. 1991; Lacey & Cole 1993), spherical and ellipsoidal collapse (e.g. Gunn & Gott 1972; Fillmore & Goldreich 1984; Bertschinger 1985; Avila-Reese et al. 1998; Sheth et al. 2001; Lu et al. 2006) and numerical simulations (e.g. Efstathiou et al. 1985; Navarro et al. 1997; Bullock et al. 2001a,b; Zhao et al. 2003a,b; Springel 2005; Macciò et al. 2007; Zhao et al. 2009). These studies have yielded the mass function, spatial distribution, formation history, and internal structure of the CDM halo population and serve as the backbone for any study of galaxy formation. The knowledge of the second stage of galaxy formation is far less well established, mainly because the baryonic processes involved (cooling, star-formation and feedback) are poorly understood. Additional physical processes whose importance is not fully understood include dynamical friction, tidal stripping, black hole formation and accretion, and adiabatic contraction.

Hydrodynamic simulations can now be used to study galaxy formation and evolution in a full cosmological context (e.g. Katz 1992; Navarro & White 1993; Kereš et al. 2005; Oppenheimer & Davé 2006; Simha et al. 2009). However, computational power is still a severe limitation at the present, and one has to compromise between simulation resolution and box size. Because of this, an alternative approach, the semi-analytical model of galaxy formation, has been developed and widely adopted to study the statistical properties of the galaxy population (e.g. White & Frenk 1991; Kauffmann et al. 1993; Mo et al. 1998; Somerville & Kolatt 1999; Avila-Reese & Firmani 2000; Cole et al. 2000; Firmani & Avila-Reese

* E-mail: luyu@stanford.edu

2000; Kang et al. 2005; Croton et al. 2006; Dutton & van den Bosch 2009). In the semi-analytical model (hereafter SAM), one adopts “recipes” to describe and parametrise the underlying physical ingredients, such as star formation and feedback. The free parameters in the models are then tuned to reproduce certain observational data of the galaxy population, such as stellar mass functions, colour-magnitude relations, metallicity-stellar mass relations, Tully-Fisher relation, and two-point statistics that describe the spatial distribution of galaxies (e.g. the two-point correlation function, the pairwise peculiar velocity dispersion, etc.). However, the theory of galaxy formation and evolution still faces several outstanding problems (see Primack 2009, for an up-to-date review). For example, it remains a challenge to fit the faint-end slope of the galaxy luminosity function (e.g. Benson & Madau 2003; Mo et al. 2005), and the models typically predict disk rotation velocities that are too high, unless adiabatic contraction and/or disk self-gravity are ignored (e.g. Cole et al. 2000; Dutton et al. 2007). In addition, the models have problems matching the evolution of the galaxy mass function with redshift (e.g. De Lucia & Blaizot 2007; Somerville et al. 2008; Fontanot et al. 2009), and typically overpredict the fraction of red satellite galaxies (Baldry et al. 2006; Weinmann et al. 2006; Kimm et al. 2009; Liu et al. 2010). There are three main reasons for these problems. First and foremost, current models most likely miss some vital ingredients or the recipes used do not properly implement the physical mechanism. Second, sub-space features and degeneracies in the model parameter space have been either missed or not sufficiently explored (Liu et al. 2010; Neistein & Weinmann 2010). Third, the difficulties may actually reflect inconsistencies in the data themselves (so-called “systematic” errors). For example, it has been pointed out that the observed evolution in the stellar mass function is inconsistent with the observed cosmic star formation history (Fardal et al. 2007; Primack et al. 2008).

To address these problems, one must quantitatively characterise the model constraints implied by existing data sets as well as explore a wider range of models. The SAM approach provides a promising avenue to tackle these problems owing to its flexibility in implementation and its relatively fast speed in computation. However, significant changes in the methodology must be made to fully utilise the potential of SAMs. The main shortcoming in current SAM implementations is that they are not probabilistically rigorous. In many published SAM applications, a subset of model parameters are held fixed while other parameters are adjusted to match some observational properties. If the match is unsatisfactory, one further adjusts some of the parameters or changes the model parametrisation until a

“good” fit is achieved. However, the goodness of fit is often assessed “by eye”; one overlays the model prediction, a luminosity function for example, on the observed result to see if the prediction is sufficiently close to the data. Since the statistical uncertainties in both the data and the model are not consistently computed, confidence levels do not follow. Similarly, since the model parameters are explored by hand, marginal probability can not be computed. As mentioned earlier, a number of physical processes in galaxy formation are still poorly understood, and so the parameterisations of these processes have to be made very general. This leaves a large parameter space to be probed. Given the high dimensionality of the parameter space and the complex covariance between parameters, it is almost impossible to find and delineate the dominant mode by hand-tuning model parameters. Third, since the model parameters might be strongly covariant, the effect of changing one model parameter is conditional to the values of other parameters that are kept fixed. Therefore, switching on and off a process in a fiducial model is unlikely to determine its importance to galaxy formation. Indeed, to investigate the influence of a specific recipe, one should allow the parameters to range over their entire a priori plausible domain and marginalise over all the other parameters. Unfortunately, this kind of analysis has not been commonly adopted owing to the lack of suitable methods. Fourth, because many processes in galaxy formation are still poorly understood, different SAMs may adopt different parameterisations for the same process. While all these models can be tuned to match a limited set of observational data and they are all considered as “plausible”, whether one model is favoured by the data more than another needs to be assessed by the marginal likelihood, instead of by the goodness-of-fit of a single optimised parameter set. To compute the marginal likelihood or evidence, all the parameters should be allowed to vary in the domain specified by the priors, so that model selection can be made according to statistical evidence. Again, such an analysis is not included in the current SAMs.

In summary, a variety of physical processes affecting galaxy formation are not yet well understood while copious observational data exist to constrain the models. Thus, to derive meaningful constraints from observations, we would like to know the probability of the various model parameters and, indeed, entire model families given the data. This leads us directly to Bayesian inference! The semi-analytical model provides a very powerful tool to translate the theory of galaxy formation into a set of model parameters. The Bayesian approach will then allow us to obtain the posterior distribution of the model parameters for a given set of data and to assess how a particular model is supported by the data. Moreover,

given different model families, Bayesian model comparison techniques such as Bayes Factors and Reversible Jump techniques (Green 1995) allow one to determine the relative odds for each model to reproduce the observed data.

Some attempts have been made recently in this direction. For instance, Bower et al. (2010) have explored the parameter space of the GALFORM model (Bower et al. 2006) using a model emulator based on Latin hypercube sampling (Mckay et al. 1979), and identified a small fraction of the initial volume of the parameter space that is not ruled out by their using the K - and b_J -band luminosity functions of galaxies in the local Universe as constraints. Using the same technique, Benson & Bower (2010) have performed an exhaustive search of model parameter space constrained by more observational data. Kampakoglou et al. (2008) and Henriques et al. (2009) have adopted the Markov-Chain Monte-Carlo (MCMC) technique to explore the ability of their adopted SAMs to accommodate multiple observational data sets.

In this paper, we develop a scheme to incorporate SAMs into the framework of Bayesian inference. To this end, we generalise the parameterisations for the model recipes so that our model can encompass the large uncertainties owing to our limited knowledge of galaxy formation. We also show that, aided with advanced MCMC techniques and moderate computational facilities, it is now possible to build a Bayesian inference-based SAM to efficiently explore the high dimensional parameter space involved and to establish the posterior distribution of model parameters reliably.

The goal of the present paper is a description of our approach and a demonstration of the advantages of a Bayesian inference-based SAM in comparison with the conventional approach. In particular, we will show that the common practise of tuning some model parameters while keeping others fixed may lead to an incorrect inference because of the use of unjustified, strong priors, and that our Bayesian inference-based SAM can overcome this problem. We will also demonstrate the sensitivity of the inference to the error model adopted for the data. The paper is organised as follows. In §2, we describe our generalised SAM and its relations to other models. A brief introduction to the principle of Bayesian inference and of the MCMC technique is presented in §3. In §4, we show a case study using the stellar mass function of galaxies as the observational constraint. The impacts of prior assumptions and data modelling on the model inference are presented in §5 and 6, respectively. Finally, in §7, we discuss and summarise our main results.

2 SEMI-ANALYTIC MODEL

As in all other SAMs, our model consists of two main parts, (i) the assembly of individual dark matter halos, and (ii) gas, radiative and star-formation processes relevant to galaxy formation. We first prepare a large set of halo merger trees with the currently favoured cosmology and adopt it for all our subsequent semi-analytical modelling of the baryonic processes. Since the formation of dark matter halos is now relatively well understood, we focus on the baryonic physics in our Bayesian analysis.

2.1 Halo merger history

Halo merger trees can either be extracted from cosmological N -body simulations (e.g. Kang et al. 2005; Croton et al. 2006), or generated by a Monte-Carlo method using the extended Press-Schechter formalism (Lacey & Cole 1993; Somerville & Kolatt 1999; Cole et al. 2000; van den Bosch 2002). Merger trees from simulations provide the dynamics and environments of the halo population, but their construction is computationally expensive and limited by numerical resolution. On the other hand, Monte-Carlo merger trees are computationally cheaper to generate and have, in principal, infinite resolution. In this paper, we adopt the algorithm proposed by Parkinson et al. (2008) to generate the merger trees for halos with a given final ($z = 0$) virial mass. This algorithm has been tuned to match the conditional mass functions found in N -body simulations. More specifically, as a demonstration we choose the control parameters $G_0 = 1$, $\gamma_1 = \gamma_2 = 0$, so that the resulting halo conditional mass functions are those predicted by the Extended Press-Schechter conditional mass function (Parkinson et al. 2008). We sample a certain number of merger trees in each halo mass bin from $10^{10} h^{-1}M_\odot$ to $10^{15} h^{-1}M_\odot$, the mass range relevant to the modelling in this paper. Since the halos and their merger trees are randomly sampled from the halo mass function and the conditional mass function, model predictions based on a finite merger tree sample suffer from sampling variance. To reduce such sampling variance, we generate a sufficiently large number of halo merger trees in each mass bin so that the variance in model predictions induced by merger-tree sampling is much smaller than the error in the observational data used to constrain the model and, hence, can be ignored. Specifically, we use 1000 merger trees for halos with present masses in the range $10^{11} - 10^{12.5} h^{-1}M_\odot$, 1500 merger trees in the range $10^{12.5} - 10^{13.5} h^{-1}M_\odot$, 400 merger trees in the range $10^{10} - 10^{11} h^{-1}M_\odot$, and about 100 merger trees in the range $10^{13.5} - 10^{15} h^{-1}M_\odot$. Since massive halos are rare

in the assumed cosmology, their contribution to the scatter of the stellar mass function is negligible. We vary the mass resolution of our merger trees with the final halo mass. For halos with final masses smaller than $10^{12} h^{-1} \text{M}_\odot$, the mass resolution is $10^{9.3} h^{-1} \text{M}_\odot$; for halos with final masses larger than $10^{14} h^{-1} \text{M}_\odot$, it is $10^{11} h^{-1} \text{M}_\odot$; and for intermediate mass halos, it is $10^{10} h^{-1} \text{M}_\odot$. All the merger trees are sampled using 60 snapshots equally spaced in $\log(1+z)$ from $z=7$ to $z=0$. Throughout the paper, we use a Λ CDM cosmology with $\Omega_{\text{M}} = 0.26$, $\Omega_{\text{B},0} = 0.044$, $h = 0.71$, $n = 0.96$, and $\sigma_8 = 0.79$, which are consistent with WMAP5 (Dunkley et al. 2009; Komatsu et al. 2009).

2.2 Radiative cooling

Once the halo formation history is fixed, we model the radiative cooling of halo gas. As shown in Lu et al. (2010), the predictions of often-used cooling models do not agree. Since these models do not incorporate uncertainties in their cooling prescriptions, the model choice imposes a strong prior on the SAM. To compare with published results, we use the cooling model of Croton et al. (2006). We will study the effects of varying the cooling prescription in a future paper. In the Croton model, the halo hot gas is redistributed at every time-step, and the density profile of the hot gas is assumed to be a singular isothermal profile,

$$\rho_{\text{gas}} = \frac{m_{\text{gas0}}}{4\pi r_{\text{vir}}} r^{-2},$$

where r_{vir} is the virial radius of the halo. The total mass of hot halo gas mass is $m_{\text{gas0}} = f_{\text{b}} m_{\text{vir}} - \sum_i [m_*^i + m_{\text{cold}}^i + m_{\text{out}}^i]$, where $f_{\text{b}} = \Omega_{\text{b}}/\Omega_0$ is the universal baryon fraction, m_* , m_{cold} and m_{out} are the masses in stars, cold gas and ejected gas, respectively, and the summation is over all galaxies in the halo. The temperature of the hot gas is constant for each halo with $T_{\text{gas}} = T_{\text{vir}} = 35.9 \left(\frac{v_{\text{vir}}}{\text{kms}^{-1}} \right)^2 \text{K}$ where v_{vir} is the circular velocity of the halo at the virial radius. The cooling timescale of the gas at radius r is then estimated by

$$\tau_{\text{cool}}(r) = \frac{3}{2} \frac{\mu m_{\text{H}} k T_{\text{gas}}}{\rho_{\text{gas}}(r) \Lambda(T_{\text{gas}}, Z_{\text{gas}})}, \quad (1)$$

where μ is the mean molecular weight in units of the mass of hydrogen atom, and Λ is the cooling function from Sutherland & Dopita (1993). At each time-step, we calculate the cooling radius r_{cool} by equating the cooling timescale with the dynamical timescale, $\tau_{\text{cool}} = \tau_{\text{dyn}} \equiv r_{\text{vir}}/v_{\text{vir}}$. If the cooling radius is equal to or smaller than the virial radius, the cooling rate is defined as

$$\dot{m}_{\text{cool}} = 0.5 m_{\text{hot}} \frac{r_{\text{cool}} v_{\text{vir}}}{r_{\text{vir}}^2}. \quad (2)$$

In other words, half of the hot gas mass enclosed by the cooling radius cools and accretes onto the central object of the halo in a dynamical timescale. If the cooling radius is larger than the virial radius, we set the cooling rate equal to the total hot gas mass in the halo divided by the dynamical timescale. We implicitly assume that all hot gas is associated with the primary halo and that only the central galaxy can accrete cooling gas; that is, satellite subhalos contain no hot gas.

In some recent SAMs, Active Galactic Nuclei (AGN) feedback reduces the gas cooling in massive halos (e.g. Croton et al. 2006; Bower et al. 2006; Somerville et al. 2008). Equivalently, AGN feedback stops radiative cooling in halos with masses larger than a characteristic mass ($\sim 10^{12} M_\odot$) (Cattaneo et al. 2006). To include this effect, we introduce a characteristic halo mass for radiative cooling, M_{CC} , above which radiative cooling of the hot halo gas is assumed to be negligible. Since the exact value of M_{CC} is not known a priori, we treat it as a free parameter in a relatively large mass range, $10^{11.5} - 10^{14.5} h^{-1} M_\odot$.

2.3 Star formation

We assume that the cooled-fraction of halo gas settles into the galaxy in an exponential disk with scale length r_{disc} . This gas forms stars when the gas disk has a surface density higher than a certain threshold, Σ_{SF} , mimicking the critical surface gas density for star formation seen in disk galaxies (e.g. Kennicutt 1998; Kennicutt et al. 2007; Bigiel et al. 2008). The fraction of cold gas above the threshold is given by the ratio of the radius r_{crit} at which the cold gas density is Σ_{SF} to the disk scale length:

$$r_{\text{crit}}/r_{\text{disc}} = \ln \frac{m_{\text{cold}}}{2\pi r_{\text{disc}}^2 \Sigma_{\text{SF}}}, \quad (3)$$

where m_{cold} is the total cold gas mass of the galaxy. Therefore, the cold gas mass enclosed by r_{crit} is determined by the ratio $r_{\text{disc}}^2 \Sigma_{\text{SF}}/m_{\text{cold}}$. Observationally, the threshold surface density is $\sim 10 M_\odot \text{pc}^{-2}$ (e.g. Martin & Kennicutt 2001), although the scale length may vary. Theoretically, the disk radius (the scale-length) is related to the virial radius and the spin parameter of its host halo: $r_{\text{disc}} \approx \frac{\lambda}{\sqrt{2}} r_{\text{vir}}$ (e.g. Mo et al. 1998). In cosmological N -body simulations, the spin parameters, λ , for dark matter halos follow a log-normal distribution with a median of ~ 0.05 (e.g. Warren et al. 1992; Cole & Lacey 1996), but the distribution of λ for the baryonic component that forms galaxy disks is poorly understood (e.g. Bett et al. 2010; Navarro & Benz 1991). In our SAM, we adopt the fiducial value $\lambda_0 = 0.05$. This yields $r_{\text{disc},0} = 0.035 r_{\text{vir}}$ and $\Sigma_{\text{SF},0} = 1 M_\odot \text{pc}^{-2}$. We then parametrise the term

$r_{\text{disc}}^2 \Sigma_{\text{SF}} = f_{\text{SF}} r_{\text{disc},0}^2 \Sigma_{\text{SF},0}$. In the Croton et al. (2006) model, r_{disc} is set to be $3r_{\text{disc},0}$, and $\Sigma_{\text{SF}} = 10 \text{ M}_{\odot} \text{pc}^{-2}$, so that $f_{\text{SF}} = 90$.

Using on our parametrisation, the cold gas mass in the disk available for star formation is

$$m_{\text{sf}} = m_{\text{cold}} \left[1 - \left(1 + \ln \frac{m_{\text{cold}}}{2\pi f_{\text{SF}} \Sigma_{\text{SF},0} r_{\text{disc},0}^2} \right) \frac{2\pi f_{\text{SF}} \Sigma_{\text{SF},0} r_{\text{disc},0}^2}{m_{\text{cold}}} \right]. \quad (4)$$

We assume that the star formation rate is proportional to the cold gas mass within r_{crit} and inversely proportional to the dynamical timescale of the disk, $\tau_{\text{disc}} = \frac{r_{\text{disc}}}{v_{\text{vir}}}$, yielding

$$\dot{m}_* = \epsilon_* \frac{m_{\text{sf}}}{\tau_{\text{disc}}}, \quad (5)$$

where ϵ_* is the star formation efficiency. We assume that ϵ_* has a broken power-law dependence on the circular velocity of the host halo:

$$\epsilon_* = \begin{cases} \alpha_{\text{SF}} & v_{\text{vir}} \geq V_{\text{SF}}; \\ \alpha_{\text{SF}} \left(\frac{v_{\text{vir}}}{V_{\text{SF}}} \right)^{\beta_{\text{SF}}} & v_{\text{vir}} < V_{\text{SF}}, \end{cases} \quad (6)$$

where α_{SF} and β_{SF} are parameters. Early models adopted a pure power-law until $\epsilon_* \sim 1$ (e.g. Kang et al. 2005). The Croton et al. (2006) model assumes $\beta_{\text{SF}} = 0$ and sets α_{SF} so that 5–15% of the cold gas is converted into stars in a disk dynamical time. The GALFORM of Cole et al. (2000) considers cases with $\beta_{\text{SF}} = 0, 1.5$ and 2.5 . In our model, all four parameters, α_{SF} , β_{SF} , V_{SF} and f_{SF} , are considered free parameters when modelling star formation in quiescent disks. It should be pointed out that our model is still based on a specific set of assumptions, even though it allows a large range of uncertainties in model parameters. There are other prescriptions for star formation that are not included in our model (e.g. Somerville et al. 2008; Krumholz et al. 2009; Fu et al. 2010).

2.4 Supernova feedback

We assume that supernova (SN) feedback affects the interstellar medium (ISM) and hot halo gas in three ways: (i) the energy feedback from SN reheats a fraction of the disk ISM from the cold phase to the hot phase, and the reheated gas is mixed with the hot halo gas; (ii) a fraction or all of the heated gas is directly ejected from the host halo without mixing with the hot halo gas; and (iii) if the SN energy from all galaxies in a halo is sufficiently large, the hot gas in the host halo can be heated, causing a fraction of the halo hot gas to be ejected from the halo. No SAM has incorporated all of these mechanisms and the strength of the feedback is usually chosen without strong prior justification. For example, the Croton

model considered both mechanisms (i) and (iii) (Croton et al. 2006), while GALFORM incorporated (i) and (ii) (Benson et al. 2003). In these models, the total amount of SN feedback energy is assumed to be related to the star formation rate, and the feedback is assumed to be instantaneous. The feedback strength is controlled by a fixed number (e.g. Croton et al. 2006) or assumed to have a power-law dependence on the circular velocity of the host halo (e.g. Somerville & Kolatt 1999; Cole et al. 2000; Kang et al. 2005). Our model incorporates all three mechanisms, and their relative strengths are free parameters. We assume that for every solar mass of stars formed, the energy released by supernovae is $\eta_{\text{sn}} E_{\text{sn}}$, where η_{sn} is determined by the stellar initial mass function (IMF) and $E_{\text{sn}} = 10^{51} \text{erg}$. Our feedback model enforces energy conservation, so that the total energy to heat the gas cannot exceed the total energy released from supernovae.

We write the SN energy released by a mass of Δm_* of star formation as

$$E_{\text{fb}} = \alpha_{\text{SN}} \frac{1}{2} \Delta m_* V_{\text{SN}}^2 \quad (7)$$

where $V_{\text{SN}} = 630 \text{km/s}$ and the free parameter α_{SN} describes the uncertainties in the feedback energy and in the IMF. For a Scalo IMF ($\eta_{\text{sn}} = 5 \times 10^{-3}$) and with 20% of the SN energy in feedback (e.g. Kang et al. 2005), we find $\alpha_{\text{SN}} = 0.25$. We allow α_{SN} to vary from 0.001 to 10, encompassing the uncertainty of this parametrisation. To conserve energy, the total SN energy released by m_* of star formation and available for feedback, E_{fb} , should be equal to the sum of the energies used for the reheating, ejection and powering the wind. Thus, we can write

$$E_{\text{fb}} = \frac{1}{2} (1 - f_{\text{ej}}) f_{\text{rh}} \Delta m_* v_{\text{vir}}^2 + \frac{1}{2} f_{\text{ej}} f_{\text{rh}} \Delta m_* v_{\text{esc}}^2 + \frac{1}{2} \Delta m_{\text{wind}} v_{\text{esc}}^2, \quad (8)$$

where the coefficients, f_{rh} and f_{ej} , control the mass loading for the reheating and ejection, v_{esc} is the circular velocity of the current host halo characterising its binding energy, and v_{vir} is the circular velocity of the host halo at the latest time when it was still a primary halo, characterising the binding energy of the galaxy. Note that $v_{\text{esc}} \neq v_{\text{vir}}$ only for satellite galaxies. We further assume that the fraction for reheating, f_{rh} , has a power-law dependence on the circular velocity of the halo, v_{vir} . If the galaxy is a satellite, we use the circular velocity of its host halo when it first became a subhalo. So we have

$$f_{\text{rh}} = \alpha_{\text{RH}} \left(\frac{V_0}{v_{\text{vir}}} \right)^{\beta_{\text{RH}}}, \quad (9)$$

where V_0 is an arbitrary factor and is set to be 220km/s . The power-law has an upper limit given by energy conservation:

$$f_{\text{rh,max}} = \alpha_{\text{SN}} \left(\frac{V_{\text{SN}}}{v_{\text{vir}}} \right)^2. \quad (10)$$

When an amount of $f_{\text{rh}} \Delta m_*$ cold gas is reheated, we assume a fraction f_{ej} escapes from the halo. For simplicity, we assume f_{ej} has a power-law dependence on the circular velocity of the current host halo:

$$f_{\text{ej}} = \alpha_{\text{EJ}} \left(\frac{V_0}{v_{\text{esc}}} \right)^{\beta_{\text{EJ}}}. \quad (11)$$

Again energy conservation sets an upper limit on f_{ej} :

$$f_{\text{ej,max}} = \left[\frac{f_{\text{rh,max}}}{f_{\text{rh}}} - 1 \right] \times \left[\left(\frac{v_{\text{esc}}}{v_{\text{vir}}} \right)^2 - 1 \right]^{-1}. \quad (12)$$

If there is still energy available after reheating and ejection, the surplus is assumed to power a wind, and the mass of the wind can be written as

$$\Delta m_{\text{wind}} = \epsilon_{\text{W}} \Delta m_* \left\{ \alpha_{\text{SN}} \left(\frac{V_{\text{SN}}}{v_{\text{esc}}} \right)^2 - f_{\text{rh}} \left[\left(\frac{v_{\text{vir}}}{v_{\text{esc}}} \right)^2 + f_{\text{ej}} \right] \right\}. \quad (13)$$

We assume that a fraction of f_{RI} of the gas in the outflow, ejection and wind will come back to the halo as hot gas in a dynamical timescale, and we treat f_{RI} as a free parameter.

Thus, we model the SN feedback with 7 parameters: α_{SN} , α_{RH} , β_{RH} , α_{EJ} , β_{EJ} , ϵ_{W} and f_{RI} . Because the wind dominates the outflow, we find that α_{EJ} and β_{EJ} are not constrained by the stellar mass function alone. Therefore, we fix $\alpha_{\text{EJ}} = 0$ and $\beta_{\text{EJ}} = 0$ in the present paper. Our model shares a number of common parameterisations with other models. For example, the reheating model is similar to the model studied in Bower et al. (2010); if α_{EJ} and β_{RH} are set to be 0, our model is reduced to the Croton model (Croton et al. 2006); if ϵ_{W} is set to be 0, our model is similar to the model described in Somerville et al. (2008). However, it is worth pointing out that other parameterisations are also possible (e.g. Benson et al. 2003).

2.5 Galaxy mergers

When two dark matter halos merge, we simply add the dark matter and hot gas of the smaller halo to the bigger one. The central galaxy of the more massive halo is then treated as the central galaxy of the new halo, and all other galaxies are considered as satellites. A satellite galaxy merges with the central galaxy in some fraction f_{DF} of the dynamical friction timescale. The dynamical friction timescale is parametrised as

$$t_{\text{fric}} = \frac{1.17 r_{\text{vir}}^2 v_{\text{vir}}}{\ln \Lambda G M_{\text{sat}}}, \quad (14)$$

where r_{vir} and v_{vir} are the virial radius and circular velocity of the new host halo, M_{sat} is the mass of the previous host halo of the satellite before it merges into the current halo, and $\ln \Lambda$

is the Coulomb logarithm, which is modelled as $\ln \Lambda = \ln(1 + M_{\text{vir}}/M_{\text{sat}})$ (e.g. Croton et al. 2006). This formula assumes that the satellite galaxy is hosted by a subhalo with mass M_{sat} and orbits in a central halo with a singular isothermal density profile of circular velocity v_{vir} , starting at the virial radius (Binney & Tremaine 1987). Earlier SAMs adopted similar parameterisations, but used different prefactors. For example, some SAMs chose the galaxy mass for M_{sat} (e.g. Cole et al. 2000) and some others chose the subhalo mass for M_{sat} (e.g. Croton et al. 2006); this results in an order of magnitude difference in the prefactor. Other uncertainties include the value of the Coulomb logarithm, the effect of tidal stripping on orbital decay, and the initial velocity of the satellite. In our model, these uncertainties are absorbed into the prefactor, f_{DF} , a free parameter.

The merging timescale is calculated when the host halo of the satellite merges into the host halo of the central galaxy. If the satellite was already a satellite before the merger, the dynamical fraction timescale for the satellite is recalculated based on the properties of the new host. When a satellite galaxy merges into the central galaxy, our treatment for the merger remnant depends on the mass ratio of the two galaxies, $m_{\text{sat}}/m_{\text{central}}$. Mergers are considered as major or minor depending on whether $m_{\text{sat}}/m_{\text{central}}$ is larger or smaller than a pre-selected $f_{\text{MG}} < 1$. The values of f_{MG} adopted in earlier SAMs are ~ 0.3 . As the choice of this parameter is not constrained by the stellar mass function of galaxies, we simply take $f_{\text{MG}} = 0.3$ instead of treating it as a free parameter.

For a minor merger ($m_{\text{sat}}/m_{\text{central}} \leq 0.3$), the satellite’s stars are added to the central bulge, and the satellite’s gas is added to the central disk. A minor merger is assumed to trigger a star-burst in the disk, and all the stars formed in the burst are added to the disk component. For a major merger ($m_{\text{sat}}/m_{\text{central}} > 0.3$), we combine all the existing stars from the two merging galaxies into a central galaxy, which is now assumed to be an elliptical. Each major merger triggers a star-burst, and all stars formed in the burst are added into the central elliptical galaxy. A fraction e_{burst} of the combined cold gas in the two merging progenitors becomes stars, and the rest joins the gaseous disk. We assume that e_{burst} depends on the ratio of the baryon masses of the two galaxies: $e_{\text{burst}} = \alpha_{\text{burst}}(m_{\text{sat}}/m_{\text{central}})^{\beta_{\text{burst}}}$.

Similar models for galaxy mergers were adopted by Somerville et al. (2001, 2008) and Croton et al. (2006) although different authors used different values for the model parameters. In our model, the four parameters in the parametrisation, f_{DF} , f_{MG} , α_{burst} and β_{burst} , are all treated as free parameters. As mentioned above, since f_{MG} is not constrained by the stellar mass function considered in this paper, we simply fix its value to be 0.3.

2.6 Calculation of a single model

The flowchart shown in Figure 1 summarises the calculation of the SAM described above. The code loads merger trees and other tables (e.g. cooling functions, stellar mass-to-light ratios for different star formation histories, and dust extinction) for subsequent calculations, and then reads the model parameters introduced above in this section, which are summarised in Table 1. We walk each merger tree from the top (the initial time) to bottom (the present time). At each tree level, a galaxy grows in the centre of a halo if the halo does not have any progenitor halos. If the halo is assembled through the mergers of progenitor halos, the central galaxy of the most massive progenitor is considered to be the central galaxy of the current halo, and all the other existing galaxies are considered to be satellites.

At the initial time, we distribute hot gas in the dark matter halos and radiative cooling begins. We sub-divide each of the 60 time steps used to sample a merger tree into 5 finer time steps (equally spaced in t) to compute the cooling and to evolve the galaxies. In every time step, gas that is able to cool in the current time step is assigned to the central galaxy. For all galaxies in the halo, star formation continues until the cold gas surface density drops below the threshold value. When a satellite galaxy merges into a central galaxy, the recipes for the morphological transformation and merger-triggered starburst are applied. For both star formation modes, quiescent or bursts, we calculate the effects of SN feedback. We model chemical evolution in the ISM using the “instantaneous recycling approximation” (Cole et al. 2000): a fraction R of the newly formed stellar mass and a yield p of heavy elements are instantaneously returned to and uniformly mixed with the cold gas. Metals enrich the halo gas as the reheated gas mixes with the hot halo gas (assuming a one-zone model, see Subsection 2.4) and affect the cooling rate. Both R and p depend on the IMF. However, since we have adopted a simplified model for gas cooling (see Subsection 2.2) and since the stellar mass function we are concerned with here is affected by metallicity only through gas cooling, in this paper we simply fix $R = 0.3$ and $p = 0.03$ instead of treating them as free parameters. Our code uses the Stellar Population Synthesis (SPS) model of Bruzual & Charlot (2003) and the dust model of Kauffmann et al. (1999) to assign fluxes to galaxies.

The evolution continues until the root of the merger tree is reached. At this point, we have a realisation of the model specified by the set of parameters. The results obtained

from these realisations can then be used to compare with observational data to evaluate the likelihood of the data given the model.

3 BAYESIAN MODEL INFERENCE AND THE MCMC METHOD

3.1 Bayesian inference

Bayes Theorem states that the posterior probability of a set of parameters Θ in a model (or hypothesis) H for given data \mathbf{D} is

$$P(\Theta|\mathbf{D}, H) \propto P(\Theta|H)L(\mathbf{D}|\Theta, H), \quad (15)$$

where $P(\Theta|H)$ is the prior probability distribution, which describes any knowledge acquired about the parameters before seeing the data, and $L(\mathbf{D}|\Theta, H)$ is the likelihood of the data \mathbf{D} for the given model parameter set Θ . As mentioned earlier, for SAMs, we have limited prior knowledge about the model parameters. Therefore, we choose either uniform or $1/x$ distributions between two physically chosen bounds for the prior distributions, depending on the particular parameter in question. As a test, the priors for some of the parameters are made strongly restrictive to demonstrate the sensitivity to these choices. Our assumed priors for the standard model (Case 0) are summarised in Table 1 as the first listed for each parameter. Note that the prior adopted for α_{SN} allows the model to use more energy to power the feedback than the total SN energy assumed to be available. With such a prior, we test whether the model could explain the data if the SN energy is somehow underestimated. The problem-specific definition of the likelihood function is described in later sections.

3.2 The Markov-Chain Monte-Carlo algorithm

Since it is not possible to integrate the posterior probability distribution function analytically for our SAM, we use a Monte-Carlo sampling approach to elucidate the posterior distribution. We adopt a newly developed software package, the Bayesian Inference Engine (BIE, Weinberg 2010a,b), which includes a suite of advanced MCMC algorithms and supports parallel computation. A detailed description of the package is beyond the scope of the present paper and can be found in the two references cited above. Here we present a brief description.

As we will show later, the topological structure of the posterior probability distribution in our problem is high-dimensional and very complex. Not only does the posterior show

#	Parameter	Meaning	Prior	Posterior
1	$\log M_{\text{CC}} (M_{\odot})$	cooling cut-off halo mass	[1.5, 4.5] [1.5, 4.5] [1.5, 4.5]	[2.19, 2.67] [3.09, 4.47] [2.13, 2.49] [3.15, 4.47] [2.07, 2.49]
2	$\log \alpha_{\text{SF}}$	star formation efficiency power-law amplitude	[-3, 0] [-3, 0] [-3, 0]	[-2.19, -0.03] [-2.97, -2.85] [-1.47, -0.03] [-2.97, -2.49]
3	β_{SF}	star formation efficiency power-law index	[-1, 12] [-0.2, 0.2] [-0.2, 0.2]	[-0.87, 0.43] [3.29, 11.87] [-0.2, 0.2] [-0.2, 0.2]
4	$\log V_{\text{SF}} (\text{km/s})$	star formation law turn-over halo circular velocity	[1.5, 3.0] [2.1, 2.3] [2.1, 2.3]	[1.52, 2.39] [2.1, 2.3] [2.1, 2.3]
5	$\log f_{\text{SF}} (M_{\odot}/\text{pc}^2)$	star formation threshold gas surface density	[-1, 3] [1.8, 2.2] [1.8, 2.2]	[-0.96, -0.64] [-0.24, 2.16] [1.8, 2.2] [1.8, 2.2]
6	$\log \alpha_{\text{SN}}$	SN feedback energy fraction	[-3, 1] [-3, 1] [-3, 1]	[-2.35, 0.85] [-1.35, -1.15] [-0.25, 1.00] [-1.75, 0.25]
7	$\log \alpha_{\text{RH}}$	SN feedback reheating power-law amplitude	[-3, 2] [-3, 2] [-3, 2]	[-2.55, 1.95] [-2.65, -0.75] [0.260, 1.22] [-0.75, 1.95]
8	β_{RH}	SN feedback reheating power-law index	[0, 14] [0, 14] [1.8, 2.2]	[0.14, 13.86] [5.46, 11.62] [1.8, 2.2]
9	$\log \epsilon_{\text{W}}$	fraction of surplus SN feedback energy used for powering wind	[-3, 0] [-3, 0] [-3, 0]	[-2.97, -0.15] [-2.97, -0.81] [-2.97, -0.21]
10	$\log f_{\text{RI}}$	fraction of re-infall ejected hot gas	[-2, 0] [-2, 0] [-2, 0]	[-1.98, -0.02] [-1.97, -0.03] [-1.94, -0.02]
11	$\log f_{\text{DF}}$	merging time-scale in dynamical friction time-scale	[-1, 2] [-1, 2] [-1, 2]	[0.53, 1.97] [0.23, 0.59] [0.77, 1.97] [0.05, 0.65]
12	$\log \alpha_{\text{SB}}$	merger triggered star burst efficiency power-law amplitude	[-2, 0] [-2, 0] [-2, 0]	[-1.98, -0.02] [-1.97, -0.09] [-1.97, -0.15]
13	β_{SB}	merger triggered star burst efficiency power-law index	[0, 2] [0, 2] [0, 2]	[0.02, 1.98] [0.02, 1.98] [0.02, 1.98]
14	α_{EJ} (fixed)	SN feedback cold gas ejection power-law amplitude	0.0	0.0
15	β_{EJ} (fixed)	SN feedback cold gas ejection power-law index	0.0	0.0
16	f_{MG} (fixed)	major merger minor merger threshold	0.3	0.3

Table 1. Summary of the model parameters. Column 2: the parameter; Column 3: the description of the parameter; Column 4: the prior distribution; Column 5: the 95% confidence bound of the posterior distribution. For the prior and posterior distributions, the three rows for each parameter are for Case 0, Case 1 and Case 2, respectively. Parameter 1 to 13 are set free, whereas parameter 14, 15 and 16 are fixed.

multi-modality and strong degeneracies among the model parameters, but also the high-probability regions only occupy a very small fraction of the entire parameter space along a curving, very thin manifold (also see Bower et al. 2010). Because of this, it is technically challenging to sample the posterior efficiently using the standard Metropolis-Hastings MCMC algorithm. To overcome this problem, we adopt differential evolution algorithm as the main algorithm for our MCMC sampler (Ter Braak 2006). For every single chain at each step, the differential evolution algorithm randomly selects two other chains and uses a fraction of the vector connecting the current states of the two chains as a proposal. This strategy improves proposal efficiency and mixing by automatically “tuning” the proposals to the ensemble of states comprising the individual chains. For a multi-dimensional Gaussian posterior, the optimised fraction of the vector is $\gamma_0 = 2.38/\sqrt{N_{\text{dim}}}$, where N_{dim} is the dimension of the parameter space (Ter Braak 2006). Since our posterior is expected to deviate significantly from a Gaussian, we use $\gamma = 0.1\gamma_0$ to maintain a good acceptance rate ($\approx 10\%$). After every 10 steps, we use the full vector as the proposal by temporally setting $\gamma = 1$ to allow the chains to swap modes. As the simulation proceeds, the chains gradually settle into the high probability regions and the distribution can guide the chains to move along the ridges of the posterior or to jump between different modes. Moreover, all the converged chains sample the posterior, further enhancing the overall efficiency.

To enhance mixing and to explore the parameter space more efficiently, we combine a tempered simulation algorithm (Neal 1996) with differential evolution. In short, tempered simulation proposes exchanges between the posterior distribution of P_0 and a “powered-up” distribution $P_j \propto P_0^{1/T_i}$ with $T_i \leq T_{\text{max}}$. Each step begins by “melting”, $T_{i+1} > T_i$ followed by “freezing”, $T_{i+1} < T_i$. We perform one tempered step for every 21 standard steps, with the maximum temperature T_{max} selected to be similar to the difference in the logarithmic posterior probability between a high-probability region and a low-probability valley: $T_{\text{max}} \approx \ln P_{\text{max}}/P_{\text{min}}$. In the temperature range from 1 to T_{max} , we set M temperature levels equally spaced logarithmically. The default value of M is set to be $\sqrt{N_{\text{dim}} + 3} \ln T_{\text{max}}$. For our problem, $N_{\text{dim}} = 13$ and we set $T_{\text{max}} = 64$, so that $M = 16$. At each temperature level T_i , 10 differential evolution steps are taken, with γ stretched by a factor of $T_i^{1/2}$. In total, it takes 320 differential evolution steps for a chain to go through the “melting” and “freezing” procedure for a single tempered step. As the parameter T_{max} controls the efficiency with which the MCMC chains explore parameter space, we have carried out tests by varying the maximum temperature. The tests show that the T_{max} we choose is sufficiently high: the

posterior does not show any new features as the temperature is increased by a factor of 4. Using a suite of tests, we also find that the tempered steps with the T_{\max} specified as above substantially improves the efficiency of exploring state space, speeding up convergence, although employing such steps significantly increases the computational load.

3.3 A Bayesian-inference based SAM

We outline the structure of our Bayesian-inference based SAM in Figure 2. The MCMC algorithm provides proposal parameter vectors for the SAM, and the SAM predicts the galaxy population using the proposed parameter set. The likelihood is evaluated by comparing the model prediction with the data, and is returned to the MCMC. The MCMC algorithm accepts or rejects the proposal based on the posterior probability and generates a new proposal for the SAM. We use our tempered differential evolution algorithm described above with 128 chains running in parallel. The MCMC-SAM loop continues until convergence is achieved. The convergence of the chains is monitored by the Gelman-Rubin \hat{R} statistic (Gelman & Rubin 1992). In essence, \hat{R} is the ratio of the variance between chains to the variance within chains. We declare convergence when $\hat{R} \leq 1.2$. When the chains are converged, we use post-convergence states (typically about 10^6) to study and characterise the posterior distribution. The converged states sample the full probability distribution of the model parameters given the observational data, and can be used to estimate confidence regions for individual model-data comparisons through marginalisation and to determine the relative posterior odds for different models. In the following sections, we use a simple example to demonstrate the power of our Bayesian-inference based SAM.

4 THE SAM POSTERIOR: STELLAR MASS FUNCTION CONSTRAINED

In this paper, we consider constraints on our SAM provided by the stellar mass function of galaxies, a fundamental property of the galaxy population that has been extensively used for model–data comparison. We choose the stellar mass function instead of the luminosity function simply because the stellar mass of galaxies is a direct prediction of our SAM, and hence we avoid problems associated with any uncertainties in the stellar population synthesis or dust models in our predictions. However, these same uncertainties are present in the reduced data, since a stellar population synthesis model was used to convert the observed galaxy luminosities into stellar masses. These uncertainties should in principle be

properly included in the error budget of the observational data. Since the purpose of this section is purely to provide a concrete demonstration of our method and to illustrate the complexities inherent in the posterior distribution function, we adopt an ad hoc model for the errors. In §6, we explore the impact of the error model on the Bayesian inference by changing our assumptions about the errors.

We study the constraints on the 13 free parameters characterising our SAM (see Table 1) using the stellar mass function of Bell et al. (2003). Assuming that stellar mass bins are mutually independent, the likelihood function is

$$L(\Phi_{\text{obs}}|\theta) = L_0 \exp \left\{ - \sum_i \frac{[\Phi_{i,\text{obs}} - \Phi_{i,\text{mod}}(\theta)]^2}{2\sigma_{i,\text{obs}}^2} \right\}, \quad (16)$$

where L_0 is an arbitrary normalisation factor, $\Phi_{i,\text{obs}}$ is the value of the observed stellar mass function in the i th bin, $\Phi_{i,\text{mod}}$ is the corresponding value predicted by the model with the given parameter set θ , and $\sigma_{i,\text{obs}}^2$ is the variance of the observed stellar mass function. The error estimation of Bell et al. (2003) only takes into account the sampling error, but we expect significant bias (systematic uncertainty) from the assumptions made in the data reduction. To mimic the effect of large systematic uncertainty, we artificially inflate the statistical error bars by a factor of 3. Please note, we are not advocating this procedure, rather, we argue this is a *very bad* thing to do in general for at least two reasons: (i) this tends to imply greater support for a model than is truly admitted by the data, and conversely, tends to reduce the ability of the data to choose between competing hypotheses; and (ii) inflated error may hide serious problems with the data or inconsistencies with other data. Strictly speaking, the Bayesian approach applies equally well to systematic uncertainty as to sampling error. Mathematically, let systematic uncertainties be described by a parameter vector η . The likelihood now depends on η through $\Phi_{i,\text{obs}}(\eta)$. We simply define a prior distribution for the uncertainty $P(\eta)$ by expert opinion or through an ancillary calibration. The inference continues as before, now with the augmented parameter vector $\Theta = (\theta, \eta)$. In the end, we simply marginalise over η . For our problem specifically, we are aware our error inflation produce is ad hoc and does not correctly represent the bin-to-bin covariance in $\Phi_{i,\text{obs}}$ induced by the stellar mass function. We will discuss how such covariance affects our results in §6. We will perform a luminosity function-based inference using a population synthesis model and an appropriately chosen prior uncertainty in a future paper. However, the lack of a stellar mass function with a suitably described error model forces us to make a crude error model approximation for the point of illustration in this section. In addition, our

Monte-Carlo evaluation of $\Phi_{i,\text{mod}}$ has variance owing to the finite sampling of the assembly histories of dark matter halos. This model dispersion should be included in the likelihood. However, it is typically 3 times smaller than the inflated error bars in the data and, therefore, not explicitly included in equation (16).

Our model also has other uncertainties. For example, the cooling rate given by different prescriptions can vary by a factor of a few (see Lu et al. 2010). Such uncertainties could be included in the likelihood evaluation if they were properly understood (e.g. Bower et al. 2010). Alternatively, one may include model uncertainties as part of the model by using an extended model family. In this paper, we restrict our demonstration to a fixed model family and ignore any uncertainties other than those represented by the priors. In a future paper we will demonstrate how to extend the analysis to multiple model families using Bayesian model selection.

We use our Tempered-Differential Evolution algorithm to run the MCMC simulation with 128 chains in parallel. The initial states of the chains are randomly distributed in parameter space according to the prior probability distribution. We terminate the simulation after 16,000 iterations, when a sufficiently large number of states are collected to summarise the marginalised posterior. The Gelman-Rubin statistic monitors the convergence of the MCMC simulation, and it identifies 123 chains that are well mixed after the simulation terminates. In Figure 3, we plot the trajectories of 3 chains randomly selected from the mixed chains and compare them with a trajectory of a outlier chain. One sees that the chains were all widely dispersed at the beginning. The mixed chains gradually converge to a high probability mode after about 3000 iterations. In contrast, the outlier chain does not converge, but wanders around in low probability regions. The simulations are kept running for 16,000 iterations, even though most of the chains have “burned-in” after 4000 iterations. For the analysis presented in this section, we take the consecutive 12,000 steps of the 123 converged chains, about 1.5 million states, to summarise the marginalised posterior probability distributions of the model parameters.

4.1 Physical implications

Figure 4 shows the one- and two-dimensional marginalised posterior probability distributions of the 13 free parameters. Three of these parameters, f_{RI} , α_{SB} and β_{SB} , are unconstrained by the stellar mass function and not shown. In the upper-right corner of the figure, we plot

the predicted stellar mass function by marginalising over the 95% confidence range of the posterior. Clearly, the stellar mass function is well reproduced by the model. Table 1 lists the 95% confidence bounds of all the parameters (as the first range listed for each parameter).

The strength of the constraints varies widely. Some parameters are weakly constrained: for example, ϵ_W , the efficiency of SN feedback powering the galactic wind, is very weakly constrained. In contrast, some parameters are tightly constrained: for example, V_{SF} is constrained to a narrow range (around $\sim 160\text{km/s}$), so are β_{SF} (around 6) and β_{RH} (around 8). Our inferred values of β_{SF} and β_{RH} are much higher than those adopted in previous SAMs. The posterior indicates a sharply suppressed star formation efficiency in halos with circular velocities below $\sim 160\text{km/s}$. In addition, the posterior distribution in the $\beta_{\text{SF}} - \beta_{\text{RH}}$ plane reveals bimodality: either the star formation efficiency or the SN reheating efficiency is a steep power-law of halo circular velocity. In other words, the shallow slope of the stellar mass function at the low-mass end requires the suppression of star formation in small halos. Since the star formation efficiency directly controls the conversion of cold gas into stellar mass, the high β_{SF} mode dominates the high β_{RH} mode. We are unsure whether or not such high values of β_{SF} and β_{RH} are physically plausible. It is likely that some new physics in addition to SN feedback is required to suppress star formation in low-mass halos, as we will demonstrate in detail in a forthcoming paper.

Some model parameters are strongly correlated. These include the following pairs of parameters: $f_{\text{SF}} - \alpha_{\text{SF}}$; $\alpha_{\text{RH}} - \beta_{\text{RH}}$; and $M_{\text{CC}} - f_{\text{DF}}$. Both α_{SF} and f_{SF} control the conversion of cold gas into stars and the degeneracy is expected. Similarly, the two parameters in the power-law parametrisation of the SN reheating, α_{RH} and β_{RH} , are degenerate. And again, the parameters controlling the two mechanisms responsible for the formation of central galaxies in massive halos, M_{CC} and f_{DF} are correlated; massive central galaxies can either acquire their mass through gas cooling and *in situ* star formation, or through the accretion of satellite galaxies. The observed sharp decline of the stellar mass function at the high-mass end requires either that gas cooling in halos more massive than $\sim 10^{12} M_{\odot}$ is effectively quenched (e.g. by AGN feedback) or that the merger rate of satellite galaxies into the central galaxy by dynamical friction is slow.

Comparing our results with those of previous studies, we notice that some of the modes we identified are broadly consistent with those found by other studies. Henriques et al. (2009) found that ϵ_{disc} in the model proposed by Croton et al. (2006), which corresponds to α_{RH} in our model, is required to be as high as about 10. Bower et al. (2010) found

that the normalisation for the star formation efficiency is as low as about 0.003, which is also similar to the mode we find for α_{SF} . Nevertheless, the features shown in the posterior distributions in these studies and ours do not generally agree because of different definitions of the parameters.

4.2 Structure of the posterior distribution

The two-dimensional posterior distributions shown in Figure 4 are marginalised over 11 dimensions and wash out much of the intrinsic sub-dimensional structure that complicates the inference and renders tweaking by hand unreliable. To demonstrate this, Figure 5 shows a 3-dimensional cut through the 13-dimensional likelihood function. The cut is made by computing the likelihood function on a fine grid of α_{SF} , α_{RH} and f_{SF} and fixing the other 10 parameters to the values where the likelihood function has its global maximum. In the plotted volume, the maximum logarithmic likelihood is $\log(L) = -3.41$, which is enclosed by the inner surface (blue) denoting $\log(L) = -4$. The outer surface (red) has $\log(L) = -9.9$. If the likelihood function were Gaussian, the outer surface would be approximately at the “1- σ ” level. The contour lines on the planes are linearly spaced in logarithm with a spacing of 13.4. The figure shows that the parameters are strongly correlated in the plotted range and that the likelihood function changes dramatically with f_{SF} . Within a small range of $\log f_{\text{SF}}$, from 1.8 to 2.0, the iso-likelihood surface moves a long distance in the $\alpha_{\text{SF}}\text{-}\alpha_{\text{RH}}$ plane and becomes elongated when $\log f_{\text{SF}}$ is close to 2.0. This type of complex structure and dramatic change happens also in the other dimensions. As a consequence, the posterior is significantly more complex than one might expect by only looking at the fully marginalised distributions presented in Figure 4. The fine structure and complex topology of the posterior also make it clear that it is extremely difficult to find the best fit by tuning model parameters by hand. It also explains why it is extremely computationally challenging to properly sample the posterior. The MCMC algorithm must navigate along extremely thin and curved surfaces in multiple dimensions, often with very small gradients in likelihood to find the most probable models. For example the results presented here required more than a million SAM evaluations with approximately 5×10^4 2GHz Opteron CPU hours.

5 THE IMPACT OF PRIOR CHOICE

In this section, we study the affect of the prior distribution on the final inference by selectively applying narrow prior distributions for some of the parameters. This mimics the common practise of fixing some model parameters. In Case 1, three of the 13 parameters are given narrow priors. The value of β_{SF} is limited to the narrow range $[-0.2, 0.2]$, to mimic a flat power-law for star formation efficiency as adopted in some SAMs (e.g. Croton et al. 2006). The parameter V_{SF} has little effect so we set $\log(V_{\text{SF}}/\text{km s}^{-1})$ in the narrow range $[2.1, 2.3]$. Furthermore, we assign a narrow prior, $[1.9, 2.1]$, to $\log f_{\text{SF}}$, corresponding to the choice $\Sigma_{\text{sf}} \approx 10 \text{ M}_{\odot}/\text{pc}^2$ and $r_{\text{disc}} \approx 3r_{\text{disc0}}$, which is often used in previous SAMs (e.g. Croton et al. 2006). All the other prior distributions are the same as in the fiducial case considered §4 (Case 0). The resulting marginalised posterior distributions in Figure 6, and summarised in Table 1 as the second prior and posterior 95% confidence range listed for each parameter, show that the distribution of all the parameters becomes more compact. The improvement of prior information on some parameters not only tightens the constraints on those parameters themselves but can also help break degeneracies in other dimensions. For example, since the star formation law is restricted to have weak dependence on halo mass, the efficiency of SN reheating is forced to be a steep power-law of halo circular velocity. For similar reasons, the degeneracies of the other parameters with β_{RH} are all also reduced. Note that this restrictive prior is not located near the dominant posterior mode with unrestricted priors (cf. Fig. 4). Moreover, the bulk of the Case 1 posterior has very low probability in the Case 0 posterior. Nevertheless, the quality of the fit does not change much, as one can see from the reproduced stellar mass function shown in the upper-right panel of Figure 6. This illustrates the danger in fixing the values of parameters to plausible values especially when there is no compelling prior reason for imposing such a strong constraint.

Case 1 requires that the SN feedback be a very steep function of the halo circular velocity when the star formation efficiency is forced to change slowly with halo mass. Early SAMs (e.g. Kauffmann et al. 1999; Kang et al. 2005) assumed a weak dependence of the SN feedback on halo mass ($\beta_{\text{RH}} \sim 2$) and concluded that the number of faint galaxies are over-predicted if $\beta_{\text{SF}} \sim 0$. However, whether or not a good fit can still be obtained by changing the other parameters while keeping $\beta_{\text{SF}} \sim 0$ and $\beta_{\text{RH}} \sim 2$ requires a full exploration of the high-dimensional parameter space. Case 2 addresses this question by imposing the additional prior restriction, $\beta_{\text{RH}} \in [1.8, 2.2]$, and in Figure 7 we show the resulting marginalised distributions,

which are summarised in the third entry for each parameter in Table 1. The modes have moved substantially with respect to those in Case 1. To compensate for the weakened SN reheating in small halos owing to the assumed weak dependence of SN reheating on halo circular velocity, the model employs a much lower efficiency for star formation and a larger reheating amplitude; the mode moves from the lower-right to the upper-left in the $\log \alpha_{\text{SF}} - \log \alpha_{\text{RH}}$ plane. For similar reasons, the posterior mode in the other dimensions also change.

The posterior-weighted stellar mass function shown in the upper-right panel of Figure 7 still reproduces the observed stellar mass function even though the power indices β_{SF} and β_{RH} are both fixed to low values. This illustrates the importance of carefully specifying the prior distribution for each parameter, especially when a parameter is weakly constrained, and the necessity for fully characterising the posterior distribution over its full domain.

In summary, the results obtained in this section show that assigning restrictive prior distributions to some parameters can significantly reduce the volume of the parameter space and tighten the constraints on all the parameters in SAMs of galaxy formation. Thus, any prior knowledge, either from observation or physical consideration, can help the model inference and hence improve our understanding of galaxy formation. However, this also indicates that full posterior distribution can be very different from the posterior distribution with restricted priors so that adopting unsubstantiated priors to fix parameters can lead to an erroneous inference for all the other parameters. Also, it would not be straightforward to estimate the potential effects of introducing additional processes when the existing model parameters are held fixed. Because of the covariance between model parameters, adding a new model parameter may change the posterior significantly.

6 IMPACT OF THE ERROR MODEL

The observational error model directly influences the value of likelihood and the shape of the cost function in parameter space. However, the impact of the error model has not been carefully considered in SAMs. In this section, we explore the effect of incorrect error estimates on the resulting inference.

Astronomers traditionally differentiate two kinds of errors, *statistical errors* and *systematic errors*. Statistical errors result from well-understood processes with known parent distributions (e.g. sampling error) while systematic errors come from the underlying assumptions made for the measurements. From the Bayesian context, a *systematic error* is

the result of poor prior information and often results in bias. For the stellar mass function considered here, the total error budget consists of the independent statistical errors of individual stellar mass bins owing to the finite number of galaxies used in estimating the stellar mass function, and systematic errors, which arise from uncertainties in the stellar population synthetic models used to estimate the stellar mass from the observed luminosity. These systematic uncertainties correlate the bins. For example, the uncertainty in the assumed IMF will increase or decrease the stellar masses of all the galaxies in the same sense.

When errors in different mass bins are correlated, the likelihood function may be approximated as follows:

$$L(\Phi_{\text{obs}}|\theta) = \frac{L_0 \exp[-\frac{1}{2}(\Phi_{\text{obs}} - \Phi_{\text{mod}})^T \cdot \Sigma^{-1} \cdot (\Phi_{\text{obs}} - \Phi_{\text{mod}})]}{(2\pi)^{I/2} |\det(\Sigma)|^{1/2}}, \quad (17)$$

where Φ_{obs} and Φ_{mod} are the vectors of the observed and predicted stellar mass functions over the stellar mass bins, Σ is the covariance matrix that describes the correlated error model, and I is the rank of the covariance matrix. For independent errors, all the off-diagonal terms vanish and the likelihood reduces to Eq.(16).

To test the effect of correlated error, we construct a synthetic stellar mass function with correlated errors that mimic the systematic uncertainties in real observation. We choose a truncated series of Chebyshev polynomials to represent the observed stellar mass function. The low-order coefficients specify the overall shape of the function, while the higher orders characterise small scale features. We find that Chebyshev polynomials up to order 4 nicely fits the logarithmic stellar mass function, $\log \Phi(\log m_*)$; the best-fit coefficients are $[-4.17, -1.26, -0.516, -0.274, -0.114]$. We choose the standard deviations of these coefficients $[0.05, 0.10, 0.12, 0.08, 0.03]$ to represent the correlated uncertainties in the measurements. Then, we calculate the covariance matrix of this synthetic data using 1000 Monte Carlo realisations of the Chebyshev polynomials and use the synthetic data and the derived covariance matrix to constrain the parameters in our SAM.

Figure 8 compares the marginalised posteriori for four pairs of model parameters obtained with the full covariance matrix (upper panels) and those obtained with the diagonal terms only (lower panels). Removing the off-diagonal terms is equivalent to ignoring the covariance. Clearly, the contours produced with the full covariance matrix are more compact. This is expected because the correlation of the errors between the different bins implies that the total independent error in the data is smaller. There are also noticeable changes in the shape and the orientation of the posterior distribution, indicating that it is important to model

the covariance of the data properly to make correct model inferences. For example, in the $\beta_{\text{SF}}\text{-log } \alpha_{\text{SF}}$ plane a new mode appears with $\log \alpha_{\text{SF}} \sim 0.5$.

7 SUMMARY AND DISCUSSION

Many of the physical processes parametrised in semi-analytical models of galaxy formation remain poorly understood and under specified. This has two critically important consequences for inferring constraints on the physical parameters: 1) prior assumptions about the size of the domain and the shape of the parameter distribution will strongly affect any resulting inference; and 2) a very large parameter space must be fully explored to obtain an accurate inference. Moreover, both *must* be done together. Both of these issues are naturally tackled with a Bayesian approach that allows one to constrain theory with data in a probabilistically rigorous way. In this paper, we have presented a semi-analytic model of galaxy formation in the framework of Bayesian inference and illustrated its performance on a test problem. Our sixteen-parameter semi-analytic model incorporates the most commonly used parameterisations of important physical processes from existing SAMs including star formation, SN feedback, galaxy merger, and AGN feedback. We combined this model with the Bayesian Inference Engine developed at the University of Massachusetts. The BIE is an extensible MPI-based software package for developing, testing and running advanced Markov-Chain Monte-Carlo algorithms on large data sets. The resulting tool allows the exploration of the posterior distribution of a large number of model parameters, and to constrain models over multiple data sets in a statistically rigorous way.

To demonstrate the power of this approach, we used the observationally derived stellar mass function of galaxies to constrain a number of important model parameters and to study the posterior probability distribution of the model parameters. The posterior probability is the conditional probability obtained after the data is taken into account. This is an important quantity for model inference because it specifies, for a given model family, the probability distribution of the parameters in the full parameter space. The Bayesian model inference requires one to examine the full posterior probability distribution, emphasising the marginalised probability instead of the ‘best’ parameters. We find that the posterior distribution has a very complex structure and topology, indicating that finding the best fit by tweaking model parameters is improbable. Moreover, the posterior clearly shows that many model parameters are strongly covariant and, therefore, the inferred value of a particular

parameter can be significantly affected by the priors used for the other parameters. As a consequence, one needs to have the knowledge about the posterior distribution in the entire parameter space when making a model inference, because it is very likely to miss significant modes if some parameters are fixed. We have demonstrated here that restricting the prior of some parameters without physical reasons can exclude models that should be considered as “plausible”, and hence lead to biased inferences. We note that the “implausibility” proposed by Bower et al. (2010) is a measure of the adequacy of a fit defined for individual parameter sets. This is different from the posterior distribution discussed here. Finally, with the use of synthetic data to mimic systematic uncertainties in the reduced data, we have shown that model parameter inferences can be significantly affected by the use of an incorrect error model. This clearly demonstrates that an accurate error model (both sampling error and systematic uncertainties) is crucial to using observational data correctly, and conversely, a data-model comparison without an accurate error model is likely to be erroneous.

The method developed here can be straightforwardly applied to other data sets and to multiple data sets simultaneously. Large galaxy surveys available now and in the near future will provide many more data sets to characterise the properties of the galaxy population not only at the present time but also at high redshifts. The Bayesian-inference based SAM described in this paper provides a framework for parameter estimation (e.g. constraining the parameters in theoretical models given particular data sets), for hypothesis testing (e.g. comparing the support for particular models given the data), and for predicting the power of new observations to constraining models of interest. In addition, the Bayesian approach explicitly builds on previous results by incorporating the constraints from previous inferences into new data sets; the Bayesian Inference Engine is designed to do this automatically. The approach developed here will produce probabilistically rigorous constraints on theoretical models, and facilitate understanding the underlying physical processes that shape the observed galaxy population. For many processes in galaxy formation, competing models have been proposed but not quantitatively compared. The marginalised likelihood or *Bayes Evidence*, which can be directly derived from the posterior, and explicit model comparison techniques, such as the reversible jump algorithm (Green 1995), can provide a quantitative comparison between different models for given data. The Bayesian hypothesis test can, therefore, be used to discriminate between models. Finally, the prediction for an observable including the inferential uncertainties can be obtained by marginalising over the posterior. Such predictions can be used to assess the power of new observations. In a series of forthcoming papers, we will use

the scheme developed here to make inferences from various data sets, focusing on a number of the aspects discussed above.

It should be pointed out, however, that the method developed here has its limitations, and improvements in the methodology are still needed to realise its full potential. For example, since the posterior is explored using MCMC sampling, one expects the computation to be more challenging as the dimensionality of the problem increases. Higher dimensionality means a larger parameter volume to be explored. If the new dimensions do not have a strong impact on the model predictions, the posterior will be extended in the new dimensions and require longer chains and/or more parallel chains to sample. If, on the other hand, the posterior is very compact in the new dimensions, the chance for a MCMC chain to find a mode will decrease. In practise, we expect the situation to be between these two extremes, but both cases make the computation more challenging. In addition, as the complexity of the model increases, one expects the topology of the posterior distribution to become more complicated, making it harder for the MCMC chains to mix well. We note that these general difficulties challenge any method of parameter space exploration, so one has to try different algorithms to determine the one that is the best suited for the problem in question. For the Tempered Differential Evolution MCMC algorithm adopted here, we may have to increase the maximum temperature for tempering to enhance mixing and/or increase the number of chains. Both of these will increase the number of SAM evaluations, each taking of order one minute to compute. One way to increase the speed of the likelihood evaluation would be to adopt a model emulator, such as the one proposed by Bower et al. (2010). However, we note that significant computation is required to train such an emulator, and that the error introduced by the emulator has to be carefully controlled.

The adding of new data to constrain the model will alter the posterior distribution. For example, the additional data may reduce the credible volume and/or produce more complex features in the posterior distribution. Except for increasing the computation time and/or improving the sampling efficiency of the algorithm as described above, the Bayesian update (e.g. Weinberg 2010b) provides a natural solution to the problem. The data-based hierarchical approach, eliciting prior information from the posterior distribution constrained by less data, allows us to update the posterior as more and more data are included into the inference. This approach may reduce the computation time significantly. On the other hand, however, it is also possible that the additional data is not mutually compatible with the old data and the main modes would change significantly. Finally, the compatibility of the model

with the two data sets, e.g. how well the model accommodates the data, should be assessed with a goodness-of-fit test.

Although the Bayesian approach is conceptually attractive, these computations are very costly. One way to increase the speed of the likelihood evaluation would be to adopt a model emulator, such as the one proposed by Bower et al. (2010). However, we note that the error introduced by the emulator has to be carefully controlled. For example, Figure 5 illustrates the complexity of the posterior distribution in parameter space. It remains to be verified that such a correlation can be accurately represented by an emulator. If the posterior distribution from the emulator approach could be used in some way to provide a prior distribution for the direct simulation, the two methods together may prove to be more powerful than either alone. Bower et al. (2010) proposed an implausibility measure to characterise the fit of the predictions to the data. Like the prior distribution, the implausibility reduces the parameter space to be explored before new data is included. This refining inference can also be accomplished by a Bayesian update, which uses the posterior obtained from part of the data as the prior for the next level of the inference that uses the remaining data.

As mentioned earlier, any model can only be considered as an approximation to reality, because of model uncertainties including stochasticity of the involved processes and inaccuracy of the model prescriptions. These uncertainties may be included in the likelihood if an assumption is made about their statistical properties. The ‘model discrepancy’ introduced in Bower et al. (2010) is an attempt along these lines. A large amount of the model uncertainties arise in SAMs because some processes are not well understood and can be modelled in various plausible ways. If a specific set of prescriptions is adopted by the model without taking into account their uncertainties, any inferences made are only for the model family specified by the adopted prescriptions. To include the model uncertainties, one can generalise the prescriptions to encompass a large number of possibilities. Alternatively, one can consider a number of plausible model families and use Bayes Evidence to discriminate between the different model families. In a forthcoming paper, we will demonstrate how the marginalised likelihood or *Bayes Evidence* can provide a quantitative comparison between different models for given data.

ACKNOWLEDGEMENTS

This material is based upon work supported by the National Aeronautics and Space Administration AISR program AISR-126270 and the National Science Foundation under Grant No. III-0611948. Disclaimer: Any opinions, findings, and conclusions or recommendations expressed in this material are those of the authors and do not necessarily reflect the views of the National Science Foundation.

REFERENCES

- Avila-Reese V., Firmani C., 2000, *Rev. Mexicana Astron. Astrofis.*, 36, 23
- Avila-Reese V., Firmani C., Hernández X., 1998, *ApJ*, 505, 37
- Baldry I. K., Balogh M. L., Bower R. G., Glazebrook K., Nichol R. C., Bamford S. P., Budavari T., 2006, *MNRAS*, 373, 469
- Bell E. F., McIntosh D. H., Katz N., Weinberg M. D., 2003, *ApJS*, 149, 289
- Benson A. J., Bower R., 2010, *MNRAS*, 405, 1573
- Benson A. J., Bower R. G., Frenk C. S., Lacey C. G., Baugh C. M., Cole S., 2003, *ApJ*, 599, 38
- Benson A. J., Madau P., 2003, *MNRAS*, 344, 835
- Bertschinger E., 1985, *ApJS*, 58, 39
- Bett P., Eke V., Frenk C. S., Jenkins A., Okamoto T., 2010, *MNRAS*, 256
- Bigiel F., Leroy A., Walter F., Brinks E., de Blok W. J. G., Madore B., Thornley M. D., 2008, *AJ*, 136, 2846
- Binney J., Tremaine S., 1987, *Galactic dynamics*. Princeton, NJ, Princeton University Press, 1987, 747 p.
- Bond J. R., Cole S., Efstathiou G., Kaiser N., 1991, *ApJ*, 379, 440
- Bower R. G., Benson A. J., Malbon R., Helly J. C., Frenk C. S., Baugh C. M., Cole S., Lacey C. G., 2006, *MNRAS*, 370, 645
- Bower R. G., Vernon I., Goldstein M., Benson A. J., Lacey C. G., Baugh C. M., Cole S., Frenk C. S., 2010, *MNRAS*, 407, 2017
- Bruzual G., Charlot S., 2003, *MNRAS*, 344, 1000
- Bullock J. S., Dekel A., Kolatt T. S., Kravtsov A. V., Klypin A. A., Porciani C., Primack J. R., 2001a, *ApJ*, 555, 240

- Bullock J. S., Kolatt T. S., Sigad Y., Somerville R. S., Kravtsov A. V., Klypin A. A., Primack J. R., Dekel A., 2001b, *MNRAS*, 321, 559
- Cattaneo A., Dekel A., Devriendt J., Guiderdoni B., Blaizot J., 2006, *MNRAS*, 370, 1651
- Cole S., Lacey C., 1996, *MNRAS*, 281, 716
- Cole S., Lacey C. G., Baugh C. M., Frenk C. S., 2000, *MNRAS*, 319, 168
- Croton D. J., Springel V., White S. D. M., De Lucia G., Frenk C. S., Gao L., Jenkins A., Kauffmann G., Navarro J. F., Yoshida N., 2006, *MNRAS*, 365, 11
- De Lucia G., Blaizot J., 2007, *MNRAS*, 375, 2
- Dunkley J., Komatsu E., Nolte M. R., Spergel D. N., Larson D., Hinshaw G., Page L., Bennett C. L., Gold B., Jarosik N., Weiland J. L., Halpern M., Hill R. S., Kogut A., Limon M., Meyer S. S., Tucker G. S., Wollack E., Wright E. L., 2009, *ApJS*, 180, 306
- Dutton A. A., van den Bosch F. C., 2009, *MNRAS*, 396, 141
- Dutton A. A., van den Bosch F. C., Dekel A., Courteau S., 2007, *ApJ*, 654, 27
- Efstathiou G., Davis M., White S. D. M., Frenk C. S., 1985, *ApJS*, 57, 241
- Fardal M. A., Katz N., Weinberg D. H., Davé R., 2007, *MNRAS*, 379, 985
- Fillmore J. A., Goldreich P., 1984, *ApJ*, 281, 1
- Firmani C., Avila-Reese V., 2000, *MNRAS*, 315, 457
- Fontanot F., De Lucia G., Monaco P., Somerville R. S., Santini P., 2009, *MNRAS*, 397, 1776
- Fu J., Guo Q., Kauffmann G., Krumholz M. R., 2010, *ArXiv e-prints*
- Gelman A., Rubin D., 1992, *Statistical Science*, 7, 457
- Green P. J., 1995, *Biometrika*, 82, 711
- Gunn J. E., Gott I. J. R., 1972, *ApJ*, 176, 1
- Henriques B. M. B., Thomas P. A., Oliver S., Roseboom I., 2009, *MNRAS*, 396, 535
- Kampakoglou M., Trotta R., Silk J., 2008, *MNRAS*, 384, 1414
- Kang X., Jing Y. P., Mo H. J., Börner G., 2005, *ApJ*, 631, 21
- Katz N., 1992, *ApJ*, 391, 502
- Kauffmann G., Colberg J. M., Diaferio A., White S. D. M., 1999, *MNRAS*, 303, 188
- Kauffmann G., White S. D. M., Guiderdoni B., 1993, *MNRAS*, 264, 201
- Kennicutt J. R. C., 1998, *ARA&A*, 36, 189
- Kennicutt J. R. C., Calzetti D., Walter F., Helou G., Hollenbach D. J., Armus L., Bendo G., Dale D. A., Draine B. T., Engelbracht C. W., Gordon K. D., Prescott M. K. M., Regan M. W., Thornley M. D., Bot C., Brinks E., de Blok E., de Mello D., Meyer M.,

- Moustakas J., Murphy E. J., Sheth K., Smith J. D. T., 2007, *ApJ*, 671, 333
- Kereš D., Katz N., Weinberg D. H., Davé R., 2005, *MNRAS*, 363, 2
- Kimm T., Somerville R. S., Yi S. K., van den Bosch F. C., Salim S., Fontanot F., Monaco P., Mo H., Pasquali A., Rich R. M., Yang X., 2009, *MNRAS*, 394, 1131
- Komatsu E., Dunkley J., Nolte M. R., Bennett C. L., Gold B., Hinshaw G., Jarosik N., Larson D., Limon M., Page L., Spergel D. N., Halpern M., Hill R. S., Kogut A., Meyer S. S., Tucker G. S., Weiland J. L., Wollack E., Wright E. L., 2009, *ApJS*, 180, 330
- Krumholz M. R., McKee C. F., Tumlinson J., 2009, *ApJ*, 699, 850
- Lacey C., Cole S., 1993, *MNRAS*, 262, 627
- Liu L., Yang X., Mo H. J., van den Bosch F. C., Springel V., 2010, *ApJ*, 712, 734
- Lu Y., Kereš D., Katz N., Mo H. J., Fardal M., Weinberg M. D., 2010, *ArXiv e-prints*
- Lu Y., Mo H. J., Katz N., Weinberg M. D., 2006, *MNRAS*, 368, 1931
- Macciò A. V., Dutton A. A., van den Bosch F. C., Moore B., Potter D., Stadel J., 2007, *MNRAS*, 378, 55
- Martin C. L., Kennicutt J. R. C., 2001, *ApJ*, 555, 301
- McKay M. D., Beckman R. J., Conover W. J., 1979, *Technometrics*, 21, 239, *American Statistical Association and American Society for Quality*
- Mo H. J., Mao S., White S. D. M., 1998, *MNRAS*, 295, 319
- Mo H. J., Yang X., van den Bosch F. C., Katz N., 2005, *MNRAS*, 363, 1155
- Navarro J. F., Benz W., 1991, *ApJ*, 380, 320
- Navarro J. F., Frenk C. S., White S. D. M., 1997, *ApJ*, 490, 493
- Navarro J. F., White S. D. M., 1993, *MNRAS*, 265, 271
- Neal R., 1996, *Statistics and Computing*, 6, 353
- Neistein E., Weinmann S. M., 2010, *MNRAS*, 405, 2717
- Oppenheimer B. D., Davé R., 2006, *MNRAS*, 373, 1265
- Parkinson H., Cole S., Helly J., 2008, *MNRAS*, 383, 557
- Press W. H., Schechter P., 1974, *ApJ*, 187, 425
- Primack J. R., 2009, in *American Institute of Physics Conference Series*, Vol. 1192, *American Institute of Physics Conference Series*, F. Roig, D. Lopes, R. de La Reza, & V. Ortega, ed., pp. 101–137
- Primack J. R., Gilmore R. C., Somerville R. S., 2008, in *American Institute of Physics Conference Series*, Vol. 1085, *American Institute of Physics Conference Series*, F. A. Aharonian, W. Hofmann, & F. Rieger, ed., pp. 71–82

- Sheth R. K., Mo H. J., Tormen G., 2001, MNRAS, 323, 1
- Simha V., Weinberg D. H., Davé R., Gnedin O. Y., Katz N., Kereš D., 2009, MNRAS, 399, 650
- Somerville R. S., Hopkins P. F., Cox T. J., Robertson B. E., Hernquist L., 2008, MNRAS, 391, 481
- Somerville R. S., Kolatt T. S., 1999, MNRAS, 305, 1
- Somerville R. S., Lemson G., Sigad Y., Dekel A., Kauffmann G., White S. D. M., 2001, MNRAS, 320, 289
- Springel V., 2005, MNRAS, 364, 1105
- Sutherland R. S., Dopita M. A., 1993, ApJS, 88, 253
- Ter Braak C. J. F., 2006, Stat. Comput., 16, 239
- van den Bosch F. C., 2002, MNRAS, 331, 98
- Warren M. S., Quinn P. J., Salmon J. K., Zurek W. H., 1992, ApJ, 399, 405
- Weinberg M. D., 2010a, The UMass Bayesian Inference Engine, <http://www.astro.umass.edu/BIE>
- Weinberg M. D., 2010b, in preparation
- Weinmann S. M., van den Bosch F. C., Yang X., Mo H. J., 2006, MNRAS, 366, 2
- White S. D. M., Frenk C. S., 1991, ApJ, 379, 52
- White S. D. M., Rees M. J., 1978, MNRAS, 183, 341
- Zhao D. H., Jing Y. P., Mo H. J., Börner G., 2003a, ApJL, 597, L9
- , 2009, ApJ, 707, 354
- Zhao D. H., Mo H. J., Jing Y. P., Börner G., 2003b, MNRAS, 339, 12

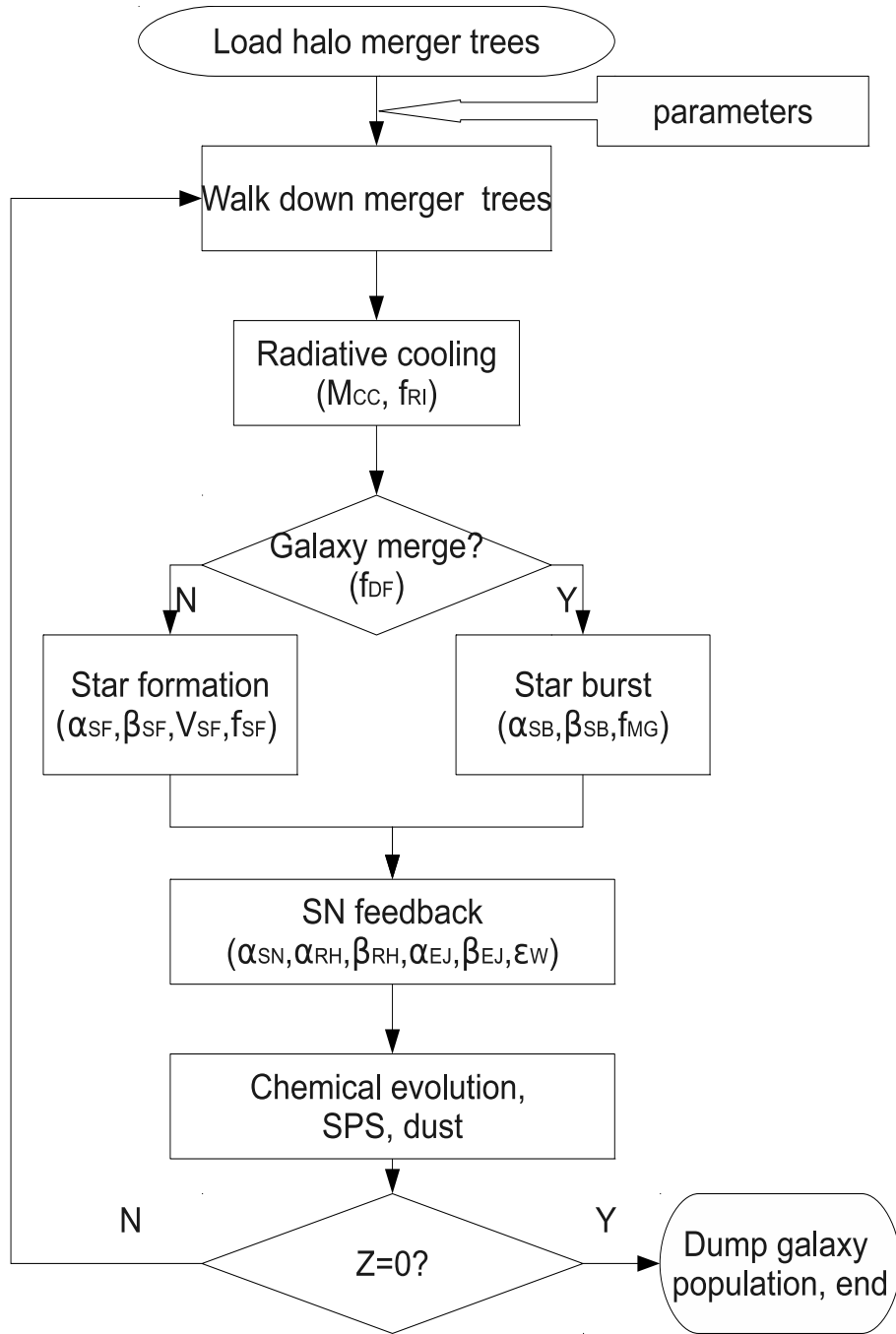


Figure 1. Flow chart describing the calculation of our semi-analytic model of galaxy formation. The parameters explored in the present paper are listed in the corresponding blocks.

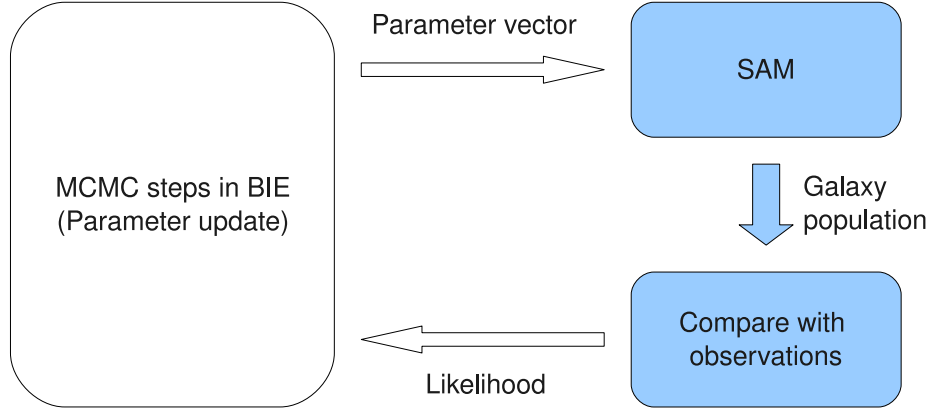


Figure 2. A flow chart describing the structure of our Bayesian-inference based semi-analytic model.

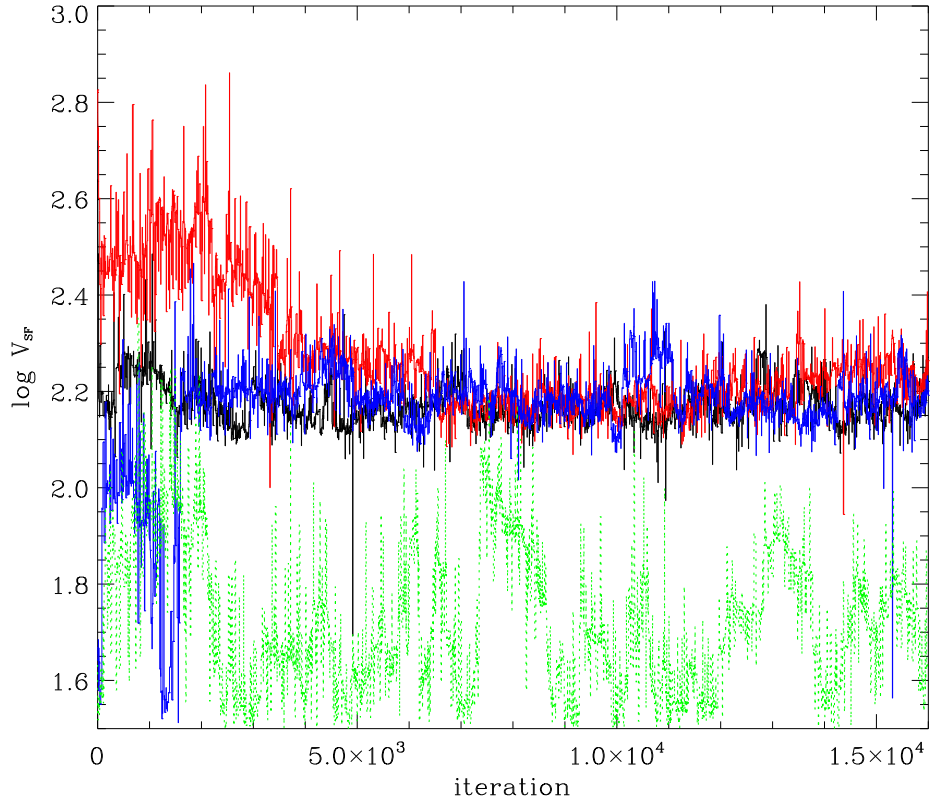


Figure 3. The trajectories of four MCMC chains run with the Tempered Differential Evolution algorithm in the dimension of the parameter V_{SF} . The three solid lines (black, red and blue) are three randomly selected converged chains, while the dotted line (green) is an outlier chain as identified by the Gelman-Rubin statistic.

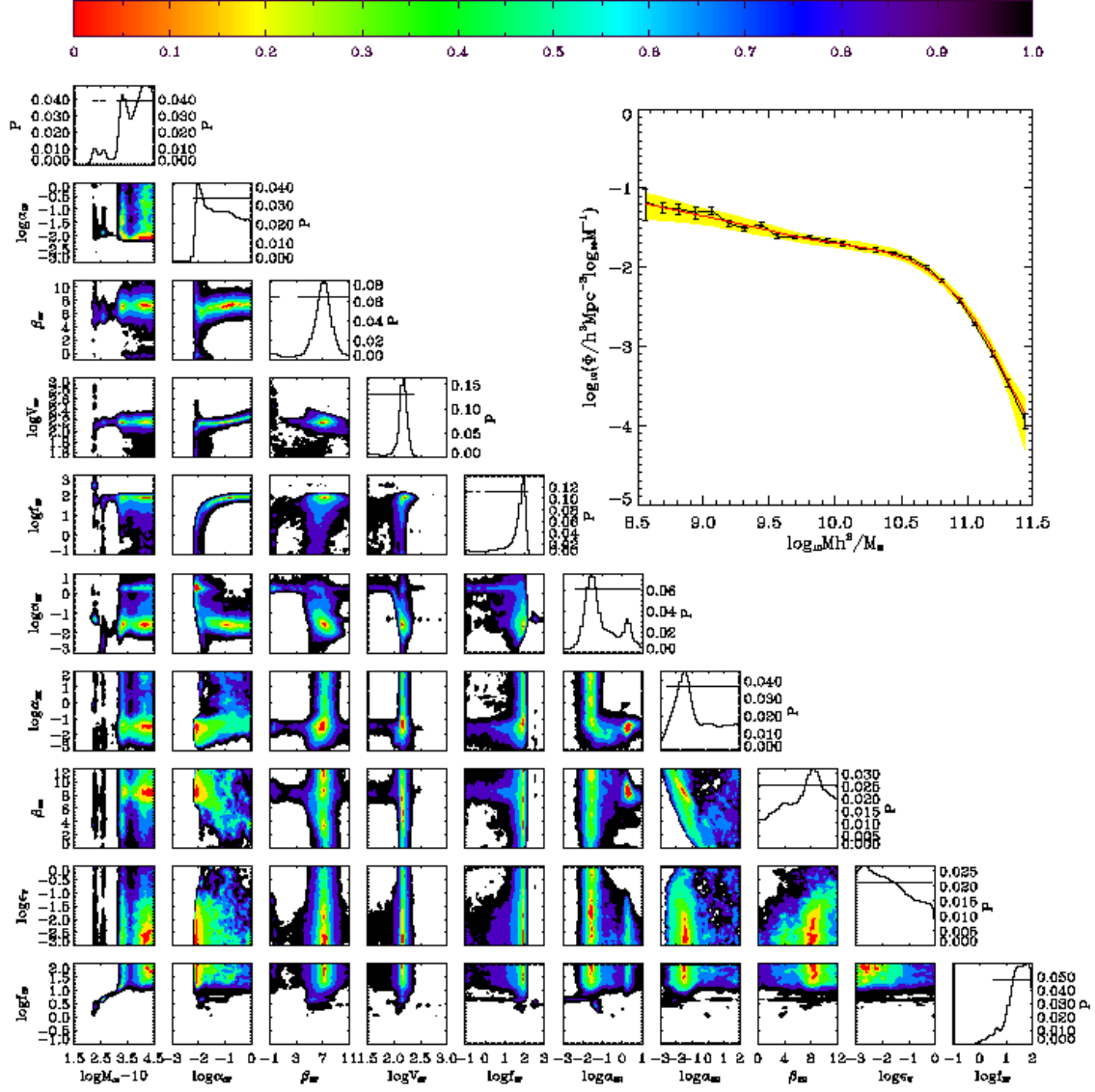


Figure 4. The marginalised posterior distribution for key parameters for our fiducial run (Case 0). The colour coding represents confidence levels as shown by the colour-bar on the top of the figure. The horizontal bars in the one-dimensional marginals indicate the 95% confidence interval. The observed stellar mass function of galaxies (black line and error bars) from (Bell et al. 2003) together with the marginalised model prediction is inset. The red solid line shows the median value of the prediction, while the yellow shaded region represents the 95% confidence interval.

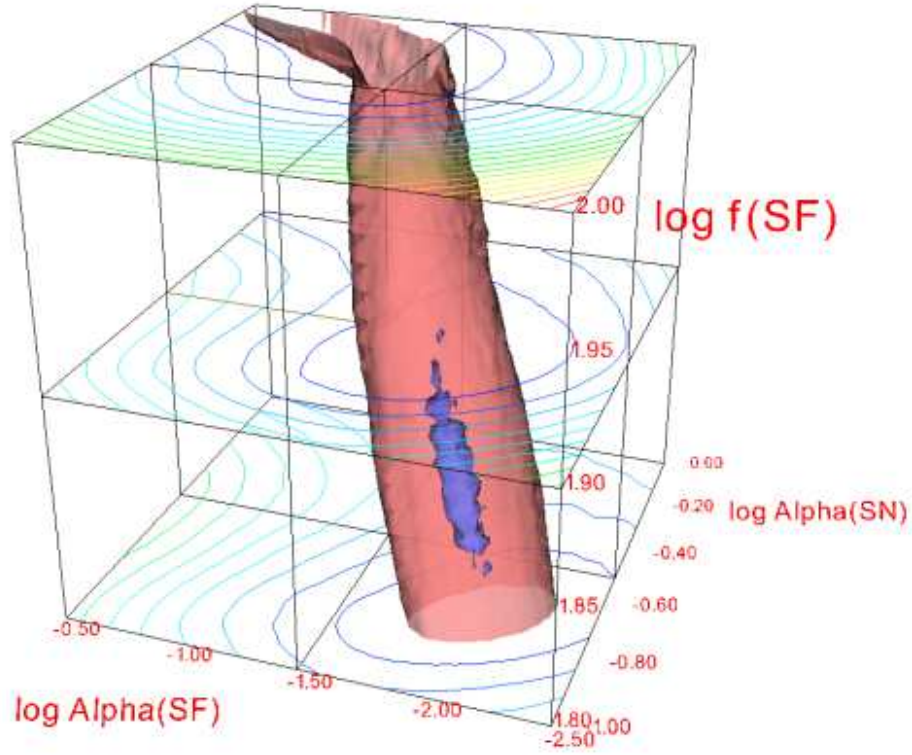


Figure 5. The likelihood function in a three-dimensional space defined by $\log \alpha_{\text{SF}}$, $\log \alpha_{\text{SN}}$ and $\log f_{\text{SF}}$. Other parameters are fixed at the values where the posterior peaks. The inner surface (blue) has $\log(L) = -4$, and the outer surface (red) has $\log(L) = -9.9$ (so the latter value is approximately “1-sigma” if the likelihood function were Gaussian). The contour lines on the planes are linearly spaced in the logarithmic scale with a spacing of 13.4. This figure demonstrates the complexity of the likelihood function and the posterior distribution.

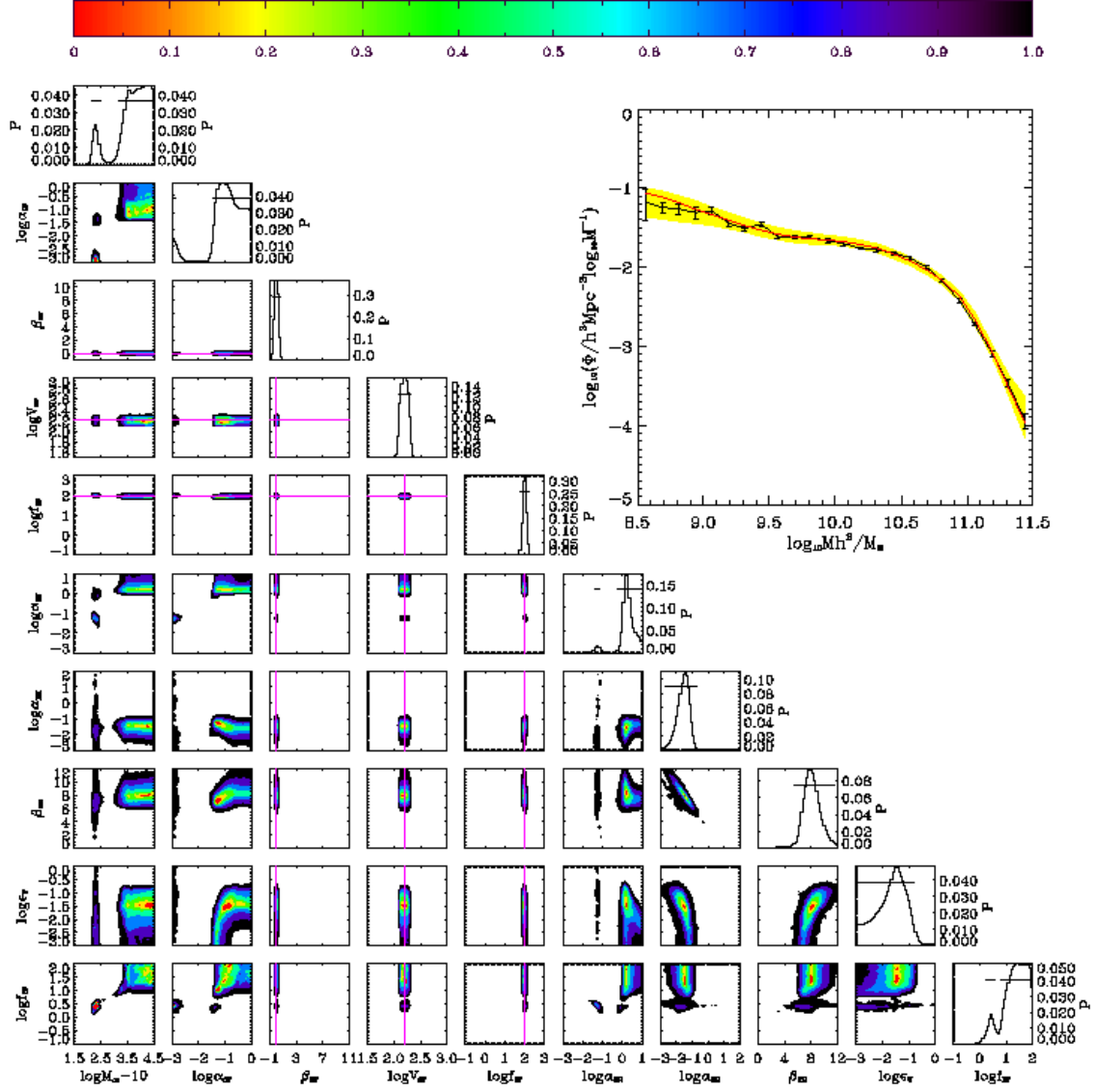


Figure 6. The marginalised posterior distribution for key parameters in Case 1. Very restrictive priors are assumed for the parameters, β_{SF} , V_{SF} and f_{SF} , whose central values are indicated by magenta lines.

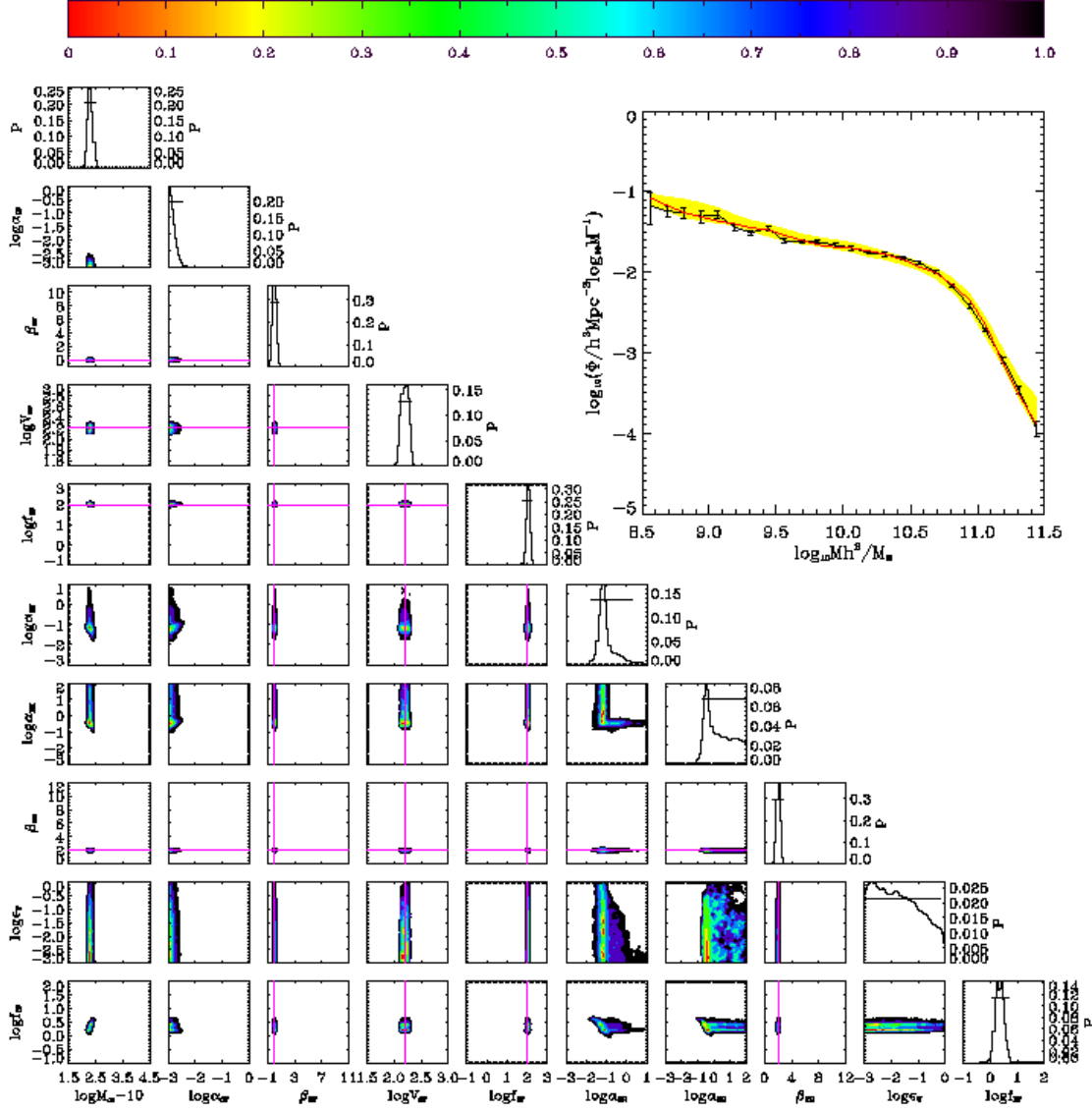


Figure 7. The marginalised posterior distribution of key parameters for Case 2. This includes the restrictions of Case 1 as in Fig. 6 with an additional restrictive prior for β_{RH} .

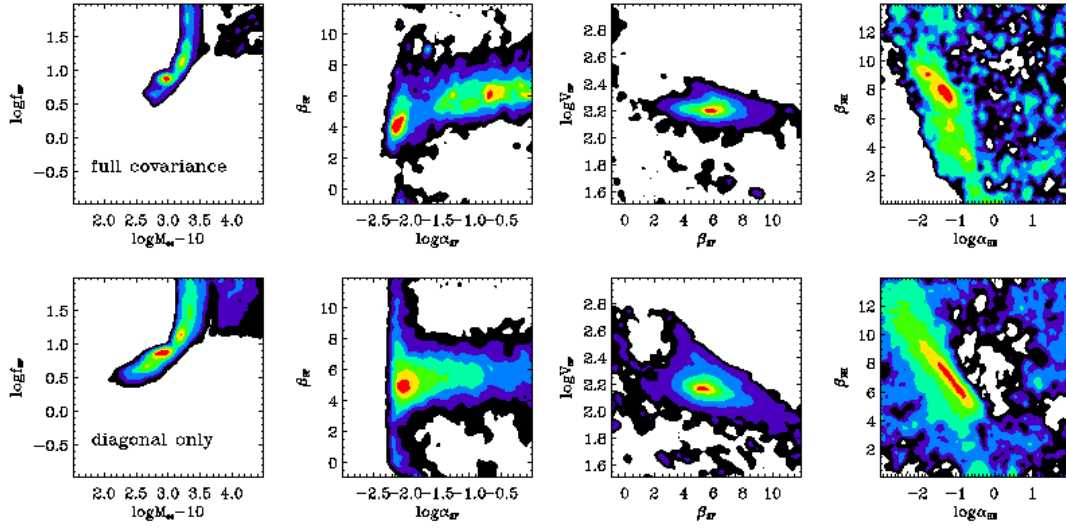


Figure 8. A comparison of the posterior distribution obtained for a likelihood function including covariance (upper row, eq. 17), and using only the diagonal terms of the covariance matrix (lower row).